ACS APPLIED MATERIALS & INTERFACES

Research Article

www.acsami.org

MoS_2-Based Nanoprobes for Detection of Silver Ions in Aqueous Solutions and Bacteria

Yu Yang,[†] Teng Liu,[‡] Liang Cheng,[‡] Guosheng Song,[‡] Zhuang Liu,*[,‡] and Meiwan Chen*[,†]

[†]State Key Laboratory of Quality Research in Chinese Medicine, Institute of Chinese Medical Sciences, University of Macau, Avenida da Universidade, Taipa, Macau, China

[‡]Institute of Functional Nano & Soft Materials Laboratory (FUNSOM), Soochow University, Suzhou, Jiangsu 215123, China

Supporting Information

ABSTRACT: Silver as an extensively used antibacterial agent also poses potential threats to the environment and human health. Hence, in this work, we design a fluorescent nanoprobe by using rhodamine B isothiocyanate (RhoBS) adsorbed MoS_2 nanosheets to realize sensitive and selective detection of Ag^+. On the surface of RhoBS-loaded MoS_2 nanosheets, Ag^+ can be reduced to Ag nanoparticles, which afterward could not only lead to the detachment of RhoBS molecules and thus their recovered fluorescence but also the surface-enhanced fluorescence from RhoBS remaining adsorbed on MoS_2. Such an interesting mechanism allows highly sensitive detection of Ag^+ (down to 10 nM) with great selectivity among other metal ions. Moreover, we further demonstrate that our MoS_2–RhoBS complex could act as a nontoxic nanoprobe to detect Ag^+ in live bacteria samples. Our work resulted from an unexpected finding and suggests the promise of two-dimensional transition-metal sulfide nanosheets as a novel platform for chemical and biological sensing.

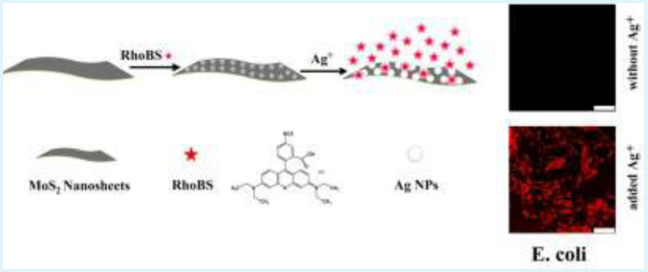

KEYWORDS: *MoS_2 nanosheets, selectivity, sensitivity, detection, bacteria*

INTRODUCTION

Silver ions (Ag^+) are able to induce significant toxic effects to algae, fungi, bacteria, and viruses. Ag-based agents have thus been widely used as antibiotics in a vast range of situations.[1−4] However, silver is regarded as a hazardous heavy metal, which can adversely affect the environment, especially water resources.[5,6] In addition, Ag^+ at high concentrations could pose risks to human health such as brain damage and disruption of the immune system.[7] Therefore, it is important to develop valid approaches for sensitive and selective determination of trace amounts of Ag^+ in both aqueous solutions and organisms.[8]

Compared with small organic molecule probes, oligonucleotide and polymer based probes, nanomaterials-based biosensors have been widely applied for the detection of nucleic acids, proteins, and metal ions because of their advantages in high specific surface area, nanometer-size effect, surface functionality, as well as intrinsic optical, electronic, and catalytic properties.[9−18] Recently, transition-metal dichalcogenides (TMDCs, e.g., MoS_2, WS_2, etc.), which are two-dimensional (2D)-layered materials analogous to graphene, have attracted extensive attention on account of their unique physical and chemical properties.[19−30] In 2013, Zhang and co-workers for the first time used MoS_2 nanosheets to construct a biosensing platform for DNA detection.[31] Later on, a number of other groups have explored the use of TMDCs for applications in detection of various biological molecules.[32−38] On the other hand, our group together with several other teams have uncovered that TMDCs with ultralarge surface area could act as a novel class of drug delivery systems promising in cancer imaging and therapy.[25,26,39] However, the application of TMDCs in the detection of heavy-metal ions in the solution phase has not yet been demonstrated to the best of our knowledge.

Herein, we designed a simple and homogeneous assay for Ag^+ detection both in aqueous solutions and living *Escherichia coli* cells by using a MoS_2-based fluorescent nanoprobe. The proposed strategy of the assay in this work is illustrated in Figure 1. Two-dimensional MoS_2 nanosheets exhibit strong optical absorbance and could act as excellent energy acceptors.

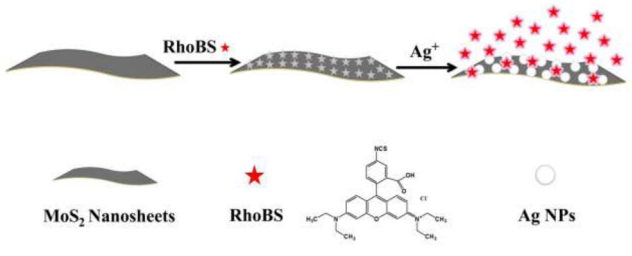

Figure 1. Schematic illustration to show the detection of Ag^+ ions using RhoBS-adsorbed MoS_2 nanosheets.

Received: December 11, 2014
Accepted: March 17, 2015
Published: March 17, 2015

DOI: 10.1021/acsami.5b01222
ACS Appl. Mater. Interfaces 2015, 7, 7526−7533

RhoBS, a photostable fluorescent dye, could be adsorbed on the surface of MoS_2 nanosheets likely via both sulfur chemistry and hydrophobic interaction,[40] leading to the effective quenching of its fluorescence via Förster resonance energy transfer (FRET). Interestingly, it is found that Ag^+ ions in the presence of MoS_2 could be rapidly reduced into Ag nanoparticles attached on the surface of MoS_2 nanosheets. As a result, the fluorescence of the MoS_2−RhoBS sample could be obviously enhanced not only because RhoBS molecules are partially replaced by AgNPs and thus show recovered fluorescence but also because the "surface-enhanced fluorescence" mechanism by which the fluorescence of RhoBS molecules remained on MoS_2 is enhanced.[41−45] While being highly sensitive with a detection limit down to ∼10 nM of Ag^+, such a MoS_2−RhoBS probe also exhibits excellent selectivity toward Ag^+ without being interfered by other tested metal ions. In situ detection of Ag^+ in *E. coli* bacteria sample is further demonstrated, highlighting the promise of our MoS_2-based sensing platform for monitoring the Ag^+ level in living organisms and investigating the antibiotic mechanism of Ag-based agents.

EXPERIMENTAL SECTION

Materials. Rhodamine B isothiocyanate and $Hg(ClO_4)\cdot 3H_2O$ were purchased from Sigma-Aldrich, and $AgNO_3$, $Al(NO_3)_3\cdot 3H_2O$, $Ba(NO_3)_2$, $MnSO_4\cdot 2H_2O$, $CaCl_2$, $Cd(SO_4)_3\cdot 8H_2O$, $CoCl_2\cdot 6H_2O$, $Cr(NO_3)_3\cdot 9H_2O$, $Cu(NO_3)\cdot 3H_2O$, KNO_3, $MgSO_4$, $Ni(NO_3)\cdot 6H_2O$, $Pb(NO_3)_2$, and $Zn(NO_3)\cdot 6H_2O$ were obtained from Sinopharm Group Co. Ltd.

Synthesis of MoS_2−RhoBS Nanosheets. MoS_2 nanosheets were synthesized by a previous method.[25,39] In a typical procedure, 500 mg of MoS_2 crystal was immersed in 0.5 mL of 1.6 M *n*-butyllithium solution in hexane for 48 h in a nitrogen glovebox. After intercalation by lithium, the MoS_2 sample was filtered and rinsed repetitiously with hexane to remove any other residuum. Intercalated MoS_2 sample was ultrasonicated in water for 1 h after being removed from the glovebox. Subsequently, exfoliated MoS_2 sample was obtained via centrifugation at 3000 rpm which could remove unexfoliated MoS_2 and excess LiOH in the precipitates. MoS_2 nanosheets were then purified by dialysis against deionized water using membranes with molecular weight cutoff (MWCO) of 14 kDa for 2 days to completely remove any residual ions.

To prepare RhoBS-modified MoS_2 nanosheets, 1 mL of MoS_2 nanosheets (1.6 μg/mL) were dispersed in the K_2CO_3 solution (pH = 8.0). One microliter of 1 mM RhoBS as-prepared solution was added into the above solution under vigorous ultrasonication for 30 min. Subsequently, mixed solutions were stirred vigorously overnight in the dark at 25 °C to allow complete adsorption of RhoBS molecules on the surface of MoS_2 nanosheets. The MoS_2−RhoBS nanosheets were centrifuged (14 800 rpm/min, 10 min) and washed three times to remove excess RhoBS molecules, obtaining MoS_2−RhoBS nanosheets stored at 4 °C for future use.

Transmission electron microscopy (TEM) images were taken by using a FEI tecnai F20 transmission electron microscope at an acceleration voltage of 200 kV. Atomic force microscopy (AFM) (Veeco Inc.) was carried out to characterize MoS_2 nanosheets. Dynamic light scattering (DLS, Marwen) was used to characterize the size and zeta potential of MoS_2 nanosheets before and after RhoBS absorption. UV−vis−NIR absorption spectra of the MoS_2 nanosheets were measured on a Perkin-Elmer UV−vis spectrophotometer. Fluorescent emission spectra were recorded with excitation at 530 nm using a FluoroMax-4 luminescent spectrometer (HORIBA JobinYvon S.A.S).

Experimental Procedures for Detection of Ag^+ Ions in Aqueous Solutions. A typical detection procedure for Ag^+ was implemented as follows. Various concentrations of Ag^+ ions solutions were prepared via serial dilution with distilled water. The as-prepared MoS_2−RhoBS nanosheets (final MoS_2 concentration = 0.8 μg/mL) were mixed with 1 mL of Ag^+ solutions with different concentrations. The mixtures were incubated in the dark for 10 min and then measured by the fluorometer under 530 nm excitation. All the measurements were performed three times. Various kinds of metal ions including Al^{3+}, Cr^{3+}, Ba^{2+}, Cd^{2+}, Cu^{2+}, Ni^{2+}, Co^{2+}, Mg^{2+}, Mn^{2+}, Pb^{2+}, Pd^{2+}, Hg^{2+}, and Zn^{2+} (100 mM in stock solutions) were diluted to definite concentrations with distilled water. For detection, 1 mL solution with 50 μM each metallic salt was incubated with the as-prepared MoS_2−RhoBS nanosheets (final MoS_2 concentration = 0.8 μg/mL). Subsequently, the fluorescence intensities of the mixed solutions were measured and analyzed using a FluoroMax-4 luminescent spectrometer (HORIBA JobinYvon S.A.S).

***E. coli* Culture and Bacteria Cell Viability Studies.** Bacteria were cultured in fresh Luria−Bertani (LB) broth at 37 °C on a shaker bed at a speed of 255 rpm until the logarithmic phase. Subsequently, the bacteria were diluted to 1×10^5 to 1×10^6 CFU/mL with fresh LB broth. Ten microliters of MoS_2−RhoBS nanosheets at different concentrations in the LB broth were added into 100 μL of bacterial suspension in each well of a 96-well microplate and incubated at 37 °C at the speed of 255 rpm overnight. After removal of materials, 100 μL of fresh LB broth and 20 μL of 3-(4,5-dimethylthiazol-2-yl)-2,5-diphenyl tetrazolium bromide (MTT) were added to the 96-well plate. The resulting precipitates were dissolved in dimethyl sulfoxide and measured under a microplate reader (Bio-Rad). All of the measurements were replicated six times for each concentration.

Cell Culture and Cell Viability Studies. 4T1, Hela, and Raw cells were obtained from American Type Culture Collection (ATCC). All cell culture reagents were purchased from Invitrogen. 4T1 and Hela Cells were cultured in a normal RPMI-1640 culture medium with 10% fetal bovine serum (FBS) and 1% penicillin/streptomycin at 37 °C in humidified air with 5% CO_2. For Row cells, high-glucose culture medium with 10% FBS, and 1% penicillin/streptomycin was supplemented.

Cell viability was determined using the standard cell viability MTT assay following the manufacturer's instruction. Briefly, 5×10^4 cells were added into each well of 96-well plates and incubated overnight. Then MoS_2−RhoBS nanosheets at various concentrations predispersed in a cell culture medium were introduced to cells and incubated for 24 h. The standard cell viability MTT assay was implemented to determine the cell viabilities relative to the control cells incubated in the medium without adding MoS_2−RhoBS nanosheets.

Intracellular Detection of Ag^+ Ions. *E. coli* cells were grown in fresh LB broth until the logarithmic phase. Ag^+ stock solutions were added into the above bacteria with the final concentrations of 20 and 50 μM. *E. coli* cells in LB broth without Ag^+ were used as a control group. After incubation for 1 h at 37 °C, Ag^+ was removed by centrifugal separation three times. Those bacteria were then incubated with 8 μg/mL of MoS_2−RhoBS nanosheets in the fresh medium for 30 min in the dark and then imaged under a Leica TCS SP5 II laser-scanning confocal fluorescence microscope.

DOI: 10.1021/acsami.5b01222
ACS Appl. Mater. Interfaces 2015, 7, 7526−7533

RESULTS AND DISCUSSION

In our experiments, MoS_2 nanosheets were prepared by exfoliating bulk MoS_2 using the Morrison method.[25,39] RhoBS molecules containing isothiocyanate group could be absorbed on the surface of two-dimensional MoS_2 nanosheets, by mixing exfoliated MoS_2 with RhoBS under ultrasonication and agitation at room temperature under pH 8.0. After being centrifuged at 14 800 rpm for 10 min and washed three times to remove excess RhoBS molecules, the MoS_2–RhoBS nanocomplex was obtained. Atomic force microscopy (AFM) (Figure 2a) imaging uncovered that chemically exfoliated

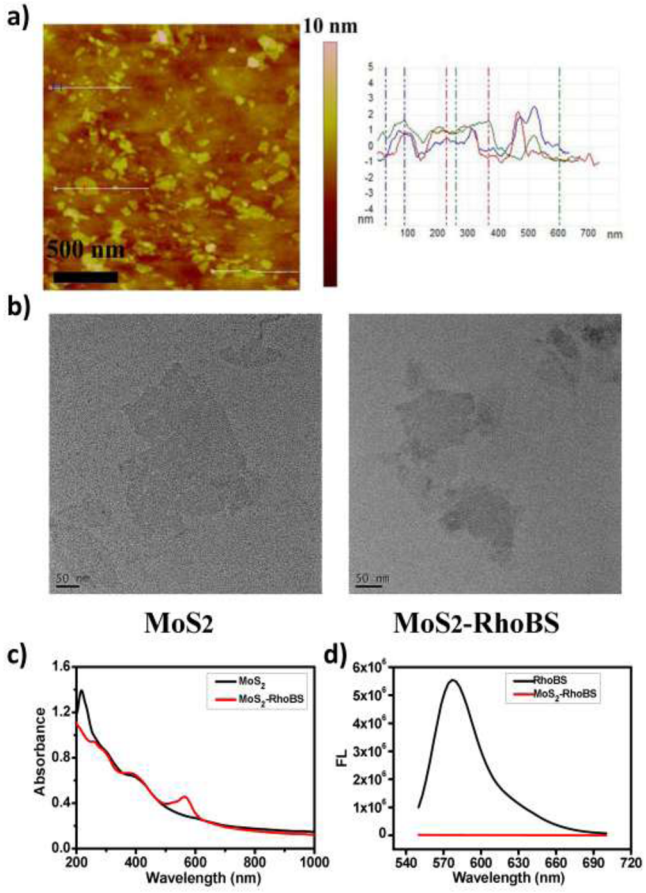

Figure 2. Characterization of MoS_2 and MoS_2–RhoB. (a) AFM images of MoS2 nanosheets. The right picture is the height profile in the AFM image. (b) TEM images of MoS_2 nanosheets before and after loading of RhoBS. (c) UV–vis spectra of MoS_2 and MoS_2–RhoBS. (d) Fluorescence emission spectra of RhoBS before and after absorption on MoS_2 nanosheets. Excitation wavelength = 530 nm.

MoS_2 nanosheets were mostly single-layered sheets. As revealed by TEM (Figure 2b) and DLS (Figure S1a,b of the Supporting Information), the sizes of MoS_2 nanosheets showed a slight decrease from ~250 to ~189 nm after loading of RhoBS, likely resulting from the ultrasonication involved in this procedure that broke down those nanosheets. On the other side, the surface charges of nanosheets remained almost the same before and after loading of RhoBS molecules (Figure S1d of the Supporting Information).

The optical properties of MoS_2 nanosheets before and after loading with RhoBS were then studied. On the basis of the absorbance spectra, while MoS_2 nanosheets showed strong absorbance from UV to near-infrared (NIR) (mass extinction coefficient = 28.4 L g^{-1} cm^{-1} at 800 nm), a RhoBS characteristic peak at ~560 nm showed up in the MoS_2–RhoBS nanocomplex after complete removal of free RhoBS (Figure 2c), indicating successful loading of RhoBS molecules onto MoS_2 nanosheets. RhoBS is a water-soluble, photostable fluorescent dye which shows robust fluorescence emission peaked at 580 nm. However, after being loaded onto MoS_2 nanosheets, the fluorescence of RhoBS was dramatically quenched (Figure 2d), indicating the presence of the FRET effect between MoS_2 nanosheets and RhoBS. To further prove the adsorption of RhoBS molecules on the MoS_2 nanosheets, Raman and infrared (IR) spectra of MoS_2 and MoS_2–RhoBS samples were measured (Figures S2 and S3 of the Supporting Information). The Raman characteristic peaks of RhoBS were observed in the MoS_2–RhoBS sample, likely owing to the surface-enhanced Raman scattering effect of MoS_2 nanosheets when RhoBS is closely attached on their surface.[46] In the meantime, two typical peaks (1385 and 2920 cm^{-1}) in the IR spectrum of the MoS_2–RhoBS sample also showed up, indicating the existence of RhoBS. Those spectroscopic data further evidenced the successful binding of RhoBS on the surface of MoS_2 nanosheets.

To test whether the fluorescence of MoS_2–RhoBS nanoprobe would be responsive to metal ions, various environmentally relevant and interfering metal ions including Al^{3+}, Ba^{2+}, Cd^{2+}, Co^{2+}, Cr^{3+}, Cu^{2+}, Hg^{2+}, Mg^{2+}, Mn^{2+}, Pb^{2+}, Pd^{2+}, Ni^{2+}, and Zn^{2+} with a concentration of 50 μM, as well as Ag^+ with a concentration of 10 μM, were mixed with MoS_2–RhoBS. We calculated the $F/F_0 - 1$ values of the solution fluorescence intensity, where F and F_0 were fluorescence intensities measured in the presence and absence of metallic ions, respectively. Interestingly, the presence of Ag^+ could lead to an obvious recovery of MoS_2–RhoBS fluorescence ($F/F_0 - 1 \approx 5$), while all the other types of metal ions even at a much higher concentration showed no appreciable impact on the MoS_2–RhoBS fluorescence (Figure 3a).

We then studied the detection kinetics and sensitivity of this assay toward Ag^+ ions in aqueous solutions. To observe the time-dependent fluorescence increase after addition of Ag^+ ions, the changes of fluorescence intensities at different time points were measured. As shown in Figure 3b, we observed that the $F/F_0 - 1$ values increased rapidly within the first 3 min after adding Ag^+ ions and reached a constant level after ~8 min. Therefore, our MoS_2–RhoBS nanoprobe showed rather rapid response to Ag^+ ions, enabling a fast detection speed. Subsequently, a series of Ag^+ solutions with different concentrations were added with equal amount of MoS_2–RhoBS nanosheets (final concentrations of MoS_2 were set be 0.8 μg/mL) to determine the detection sensitivity. We found that the fluorescence intensities at 580 nm increased gradually with the increase of Ag^+ ion concentrations (Figure 3c). As shown in Figure 3d, a linear relationship between the fluorescence intensities and logarithmic concentrations of Ag^+ was observed in the Ag^+ concentration range from 10 to 500 nM. The limit of detection of this assay appeared to be as low as 10 nM, which was much lower than the maximum level (0.46 μM) of silver in drinking water licensed by the U.S. Environmental Protection Agency (U.S. EPA).

Next, we investigated how Ag^+ rather than other metal ions could induce the recovery of fluorescence from RhoBS adsorbed on the surface of MoS_2 nanosheets. First, we obtained the TEM image to characterize MoS_2–RhoBS nanosheets after the addition of Ag^+. As shown in Figure 4a, we noted that

DOI: 10.1021/acsami.5b01222
ACS Appl. Mater. Interfaces 2015, 7, 7526–7533

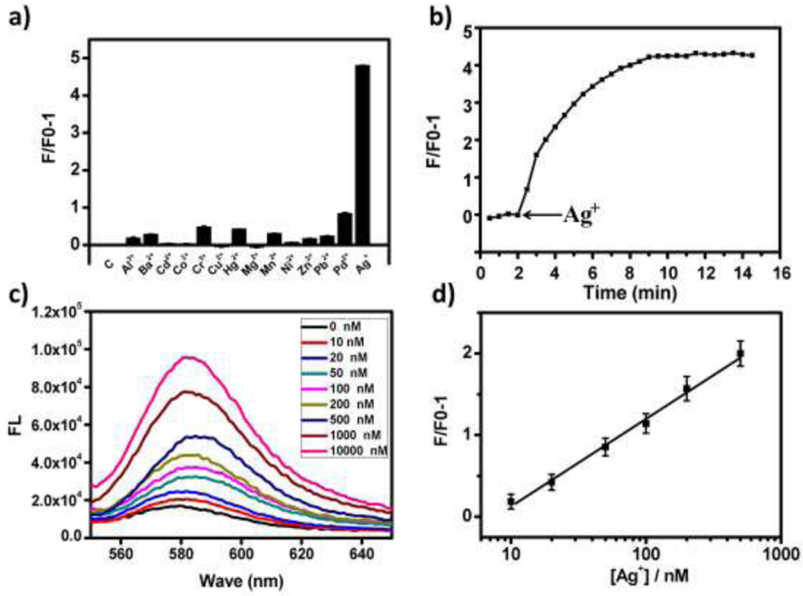

Figure 3. MoS_2–RhoBS nanoprobe for Ag^+ detection in aqueous solutions. (a) Selectivity analysis for Ag^+ detection. Bars represent the enhanced fluorescence ratio ($F/F_0 - 1$) of MoS_2–RhoBS (0.8 μg/mL) solutions in the presence of 50 μM interfering metal ions and 10 μM Ag^+ ions. (b) The enhanced fluorescence ratio ($F/F_0 - 1$) of MoS_2–RhoBS vs time upon addition of 10 μM Ag^+. (c) The fluorescence emission spectra of MoS_2–RhoBS (0.8 μg/mL) solutions taken after adding various concentrations of Ag^+ ions from 10 nM to 10 μM. (d) The plot of fluorescence intensity at 580 nm versus the increasing concentrations of Ag^+ ions in the MoS_2–RhoBS solutions. Excitation wavelength = 530 nm.

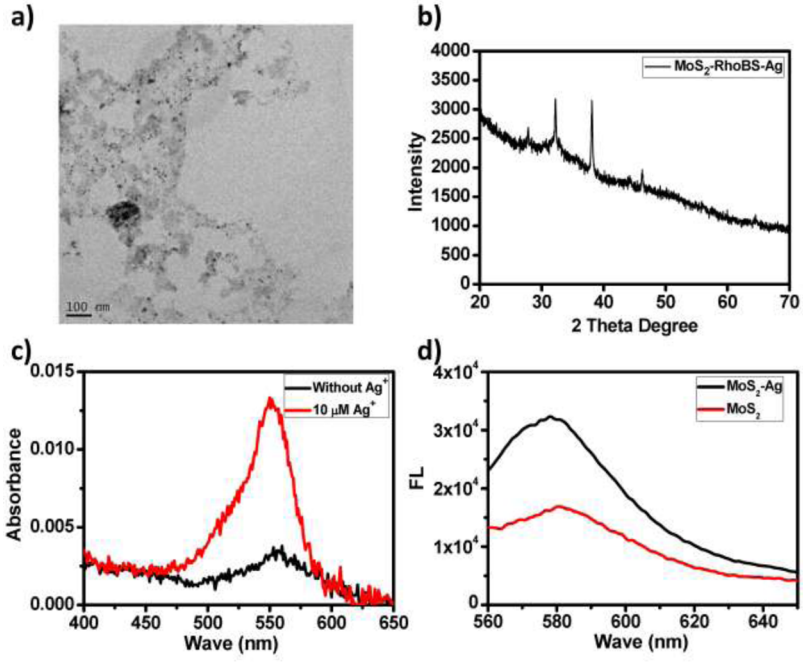

Figure 4. (a) TEM image of MoS_2–RhoBS after incubation with Ag^+. Many nanoparticles were found on those nanosheets. (b) X-ray diffraction (XRD) patterns of MoS_2–RhoBS after incubation with Ag^+. (c) UV–vis spectra of released RhoBS from MoS_2–RhoBS in the supernatant solutions with (red line) and without (dark line) incubating MoS_2–RhoBS (0.8 μg/mL) with 10 μM Ag^+ ions. (d) The fluorescence emission spectra of RhoBS added with MoS_2 or MoS_2–Ag complex.

abundant nanoparticles were adsorbed on the surface of MoS_2 nanosheets after mixing MoS_2–RhoBS with Ag^+. Those nanoparticles were further confirmed to be Ag nanoparticles by X-ray diffraction (XRD) (Figure 4b). The characteristic peaks at 38.2°, 44.3°, and 64.5° in the XRD pattern could be reflected from the (1 1 1), (2 0 0), and (2 2 0) crystallographic planes of Ag nanoparticles with face-centered cubic structure (JCPDS No. 04-0783).

Subsequently, we speculated whether it was the release of RhoBS molecules during the formation of AgNPs on MoS_2 nanosheets that resulted in the fluorescence recovery. To check if there was any release of RhoBS from MoS_2–RhoBS after addition of Ag^+, MoS_2–RhoBS was incubated with 10 μM Ag^+ ions and then collected by centrifugation at 148 000 rpm for 10 min. The released RhoBS in the supernatant solution was measured by UV–vis spectra (Figure 4c). While RhoBS

DOI: 10.1021/acsami.5b01222
ACS Appl. Mater. Interfaces 2015, 7, 7526–7533

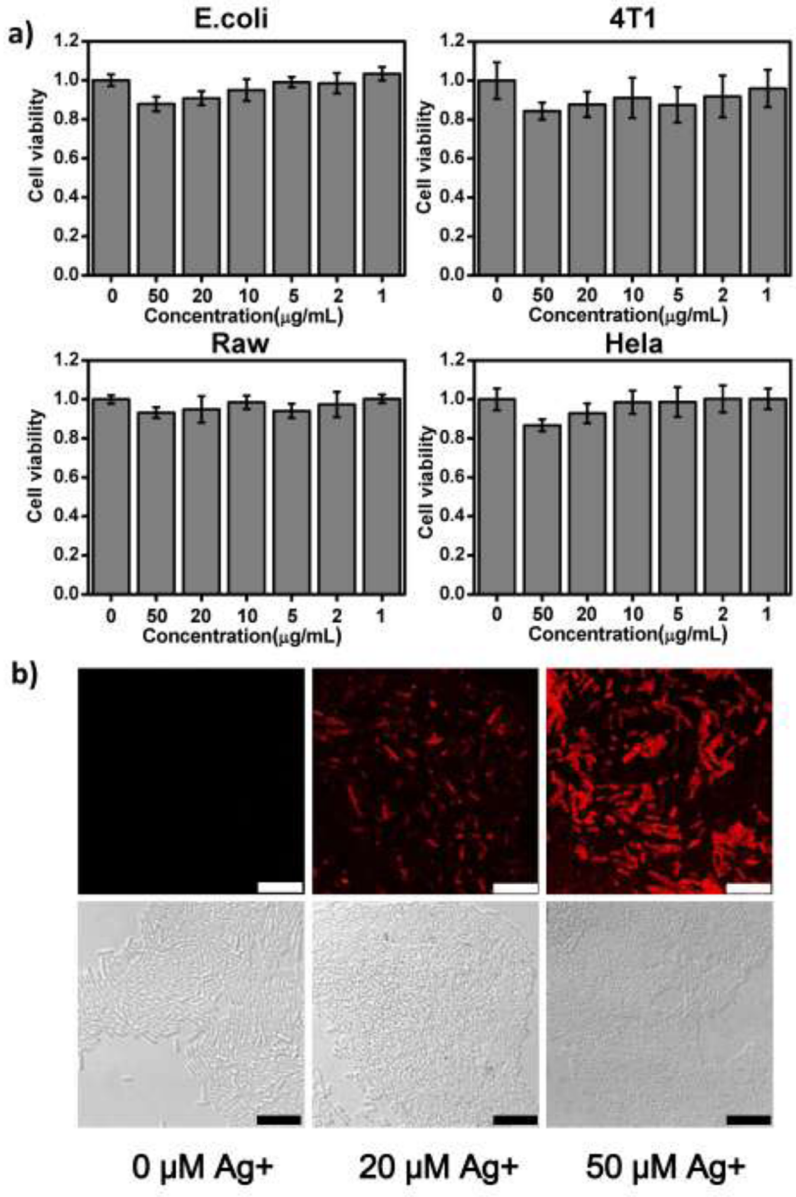

Figure 5. Intracellular Ag^+ detection. (a) Cell viabilities of *E. coli*, 4T1, Raw, and Hela cells exposed to various concentrations of MoS_2−RhoBS nanosheets for 24 h. (b) Confocal fluorescence images of *E. coli* stained with MoS_2−RhoBS nanoprobe. In this experiment, *E. coli* were cultured with 0, 20, or 50 μM Ag^+ ions, washed by LB medium, and then added with MoS_2−RhoBS (8 μg/mL) before imaging. The observed fluorescence came from recovered RhoBS fluorescence of our nanoprobe. Scale bar = 7.5 μm.

molecules were stably adsorbed on MoS_2 nanosheets in the absence of Ag^+ ions, an obvious RhoBS absorbance peak was noted in the supernatant solution from the Ag^+ incorporated MoS_2−RhoBS sample, suggesting that addition of Ag^+ and the subsequent formation of Ag nanoparticles on MoS_2 could indeed induce the detachment of RhoBS molecules from nanosheets surface, and thus the recovery of RhoBS fluorescence.

It is well-known that the surface plasmon resonance on nobel-metal surface could induce a surface-enhanced fluorescence (SEF) effect, which is able to enhance the fluorescence intensity of nearby fluorophore.[42−45] It is therefore possible that Ag nanoparticles formed on the surface of MoS_2 may be able to enhance the fluorescence of RhoBS which remained on the surface of MoS_2. To check this possibility, MoS_2 nanosheets were added with 10 μM as-prepared Ag^+ solutions to form MoS_2−Ag complexes. One microliter of 1 mM RhoBS was separately added into MoS_2 and MoS_2−Ag solutions (with the same concentration of MoS_2). The fluorescence intensities of those mixtures were then measured. As shown in Figure 4d, an obvious fluorescence enhancement effect was observed for the MoS_2−Ag−RhoBS sample, indicating that Ag nanoparticles formed on the surface of MoS_2 could enhance the fluorescence of RhoBS molecules via SEF.

Several nanosensors exhibit great potential for Ag^+ ions detection; however, many of them work well only in the aqueous solution.[47,48] To study the possibility for monitoring Ag^+ ion levels in living organisms, we used MoS_2−RhoBS nanosheets as a nanosensor to detect Ag^+ ions in *E. coli*, a Gram-negative bacterium. First, we tested the stability of Rhodamine B isothiocyanate−MoS_2 complex in the water, PBS, and culture medium. After 12 h, RhoBS−MoS_2 complex

DOI: 10.1021/acsami.5b01222
ACS Appl. Mater. Interfaces 2015, 7, 7526−7533

Table 1. Detection Mechanism, Sensitivity, and Practicability of Various Nanosensors for Detection of Ag^+ Ions

materials	detection mechanism	sensitivity	applications	references
MoS_2−RhoBS nanocomplex	Ag^+ was reduced to Ag NPs, leading to fluorescence recovery of RhoBS	10 nM	in aqueous solution and living bacteria	this work
Au nanoparticles	surface-enhanced Raman scattering (SERS)	25 nM	in pool water	49
Fe_3O_4@Au nanoparticles	selective magnetic electrochemical method	59 nM	in aqueous solution	50
gold nanorods	Ag^+ changes the longitudinal plasmon wavelength (LPW) of gold nanorods	10 nM	in aqueous solution	51
$Au(S_2O_3)_2^{3-}$ core−shell nanoparticles	plasmon-derived optical resonance adjusted with controllable core−shell nanoparticles	10 nM	in aqueous solution	52
CdSe quantum dots	quenching of CdSe fluorescence signal	70 nM	in aqueous solution	53
ZnS:Mn/ZnS@ iminodiacetic acid	iminodiacetic acid of QDs-IDA and Ag^+ ions complex promoted the photoinduced electron transfer	260 nM	in aqueous solution	54
Tween 20-AuNPs	Ag^+ on the Au surface lead to AuNPs aggregation	100 nM	in drinking water	55
FAM-ssDNA-graphene oxide	The chelation action between Ag^+ ions and G-rich FAM-ssDNA	50 nM	in aqueous solution	56

appeared to be highly stable without aggregation in all of those physiological solutions (Figure S4 of the Supporting Information). We then investigated the potential cell toxicity of this nanoprobe. *E. coli*, together with several mammalian cell lines (4T1, Raw, and Hela cells), were incubated with various concentrations of MoS_2−RhoBS nanosheets (maximum concentration at 50 μg/mL) for 24 h. The cell viability assay by using 3-(4,5-dimethylthiazol-2-yl)-2,5-diphenyltetrazolium bromide (MTT) showed that MoS_2−RhoBS nanosheets had no obvious toxicity in vitro even at our highest tested concentration, which was over 6 times higher than the concentration used in the Ag^+ detection (Figure 5a).

Subsequently, we detected the intracellular Ag^+ ions in living *E. coli* cells. *E. coli* cells were incubated with 0, 20, and 50 μM of Ag^+ for 1 h. After extracellular Ag^+ ions were removed, MoS_2−RhoBS nanosheets (8 μg/mL) in the LB medium were added into *E. coli* cells for incubation of 30 min. TEM images of bacteria cell slices revealed that MoS_2 nanosheets were able to enter those bacteria cells (Figure S5 of the Supporting Information). Thereafter, fluorescence detection of Ag^+ ions in living bacteria was conducted by using a laser-scanning confocal fluorescence microscope. Without pretreatment of Ag^+ ions, *E. coli* cells showed no appreciable fluorescence. While in the presence of Ag^+ ions, *E. coli* cells exhibited significant fluorescence originating from RhoBS. Moreover, the fluorescence intensity of bacteria was enhanced with the increase of Ag^+ ion concentration used during pretreatment (Figure 5b). Our results indicated that this assay is particularly suitable for detection of Ag^+ ions in the organisms. Since Ag^+ has the capability of killing bacteria and has been widely used as an antibacterial agent, our sensor may be useful to investigate the bacteria-killing mechanism of Ag-based antibiotic agents.

Compared with other nanomaterials such as gold nanostructures and graphene nanosheets as fluorescence quenching substrate, MoS_2 nanosheets could intrinsically induce the reduction of Ag^+ to Ag nanoparticles on the surface of MoS_2 nanosheets due to the S atoms on the surface of MoS_2, which may serve as the reducing agent to enable the formation of AgNPs, enabling direct detection of Ag^+ via the fluorescence recovery of Rhodamine B isothiocyanate. This system is simple and easy to prepare for sensitive and selective detection of sliver ions in aqueous solutions and also applicable to the living systems as demonstrated by the imaging of Ag^+ in bacteria. In terms of detection sensitivity and practicability, the comparison of our probe with other previously reported nanosensors have been listed in Table 1. Our system offers comparable or higher sensitivity compared to other previously reported nanosensors for Ag^+ detection.

CONCLUSION

In summary, we have reported a nanosensor based on dye-adsorbed MoS_2 nanosheets for ultrasensitive and selective detection of Ag^+ ions both in aqueous solutions and living *E. coli* cells. In this assay, Ag^+ was reduced to Ag nanoparticles on the MoS_2 nanosheets, which could not only lead to the replacement of RhoBS molecules and thus their recovered fluorescence but also the result in surface-enhanced fluorescence from RhoBS remaining adsorbed on MoS_2. Such nanosensor platform is a simple, precise, and easily operated method which can be accomplished within 10 min. Moreover, this method displays a linear concentration range of Ag^+ from 10 to 500 nM with a rather low detection limit down to 10 nM. More importantly, our nanoprobe, while being nontoxic to bacteria and mammal cells, is able to monitor Ag^+ ions level in/on living *E. coli* cells. The capability of detecting Ag^+ in living organisms could potentially allow us to better understand the antibiotic mechanism of many Ag-based antibacterial agents. Moreover, our work highlights the promise of using 2D TMDC materials to construct novel nanoprobes for chemical and biological sensing.

ASSOCIATED CONTENT

Supporting Information

Additional characterization data of MoS_2−RhoBS nanosheets, including size distributions and zeta potential of MoS_2−RhoBS nanosheets; photos of MoS_2−RhoBS nanosheets in water, PBS, and culture medium; Raman spectra and infrared spectra; TEM images of *E. coli* cells incubated with MoS_2−RhoBS complex. This material is available free of charge via the Internet at http://pubs.acs.org/.

AUTHOR INFORMATION

Corresponding Authors

*E-mail: MWChen@umac.mo.
*E-mail: zliu@suda.edu.cn.

Notes

The authors declare no competing financial interest.

ACKNOWLEDGMENTS

This work was partially supported by the National Natural Science Foundation of China (51222203, 51132006), the National "973" Program of China (2011CB911002, 2012CB932601), a Jiangsu Natural Science Fund for Distinguished Young Scholars, the Macao Science and Technology Development Fund (062/2013/A2), and the

DOI: 10.1021/acsami.5b01222
ACS Appl. Mater. Interfaces 2015, 7, 7526−7533

Research Fund of the University of Macau (MYRG2014-00033-ICMS-QRCM, MYRG2014-00051-ICMS-QRCM).

REFERENCES

(1) Caruso, D. M.; Foster, K. N.; Hermans, M. H.; Rick, C. Aquacel Ag (R) in the Management of Partial-Thickness Burns: Results of a Clinical Trial. *J. Burn Care Res.* **2004**, *25*, 89−97.

(2) Secinti, K. D.; Özalp, H.; Attar, A.; Sargon, M. F. Nanoparticle Silver Ion Coatings Inhibit Biofilm Formation on Titanium Implants. *J. Clin. Neurosci.* **2011**, *18*, 391−395.

(3) Silver, S. Bacterial Silver Resistance: Molecular Biology and Uses and Misuses of Silver Compounds. *FEMS Microbiol. Rev.* **2003**, *27*, 341−353.

(4) Silver, S.; Lo, J.; Gupta, A. Silver Cations as an Antimicrobial Agent: Clinical Uses and Bacterial Resistance. *APUA Newsletter* **1999**, *17*, 1−3.

(5) Lo, S. F.; Hayter, M.; Chang, C. J.; Hu, W. Y.; Lee, L. L. A Systematic Review of Silver-Releasing Dressings in the Management of Infected Chronic Wounds. *J. Clin. Nurs.* **2008**, *17*, 1973−1985.

(6) Ceresa, A.; Radu, A.; Peper, S.; Bakker, E.; Pretsch, E. Rational Design of Potentiometric Trace Level Ion Sensors. A Ag^+-Selective Electrode with a 100 ppt Detection Limit. *Anal. Chem.* **2002**, *74*, 4027−4036.

(7) Eisler, R. *Silver Hazards to Fish, Wildlife, and Invertebrates: A Synoptic Review; DTIC Document*; Contaminant Hazard Reviews, Report 32; U.S. Department of the Interior, National Biological Service: Laurel, MD, 1996.

(8) Singha, S.; Kim, D.; Seo, H.; Cho, S. W.; Ahn, K. H. Fluorescence Sensing Systems for Gold and Silver Species. *Chem. Soc. Rev.* **2015**, DOI: 10.1039/C4CS00328D.

(9) Liu, D.; Wang, S.; Swierczewska, M.; Huang, X.; Bhirde, A. A.; Sun, J.; Wang, Z.; Yang, M.; Jiang, X.; Chen, X. Highly Robust, Recyclable Displacement Assay for Mercuric Ions in Aqueous Solutions and Living Cells. *ACS Nano* **2012**, *6*, 10999−11008.

(10) Li, J.; Song, S. P.; Liu, X. F.; Wang, L. H.; Pan, D.; Huang, Q.; Zhao, Y.; Fan, C. H. Enzyme-Based Multi-component Optical Nanoprobes for Sequence-Specific Detection of DNA Hybridization. *Adv. Mater.* **2008**, *20*, 497.

(11) Hu, M.; Yan, J.; He, Y.; Lu, H. T.; Weng, L. X.; Song, S. P.; Fan, C. H.; Wang, L. H. Ultrasensitive, Multiplexed Detection of Cancer Biomarkers Directly in Serum by Using a Quantum Dot-Based Microfluidic Protein Chip. *ACS Nano* **2010**, *4*, 488−494.

(12) Zhao, C.; Qu, K. G.; Song, Y. J.; Xu, C.; Ren, J. S.; Qu, X. G. A Reusable DNA Single-Walled Carbon-Nanotube-Based Fluorescent Sensor for Highly Sensitive and Selective Detection of Ag^+ and Cysteine in Aqueous Solutions. *Chem.—Eur. J.* **2010**, *16*, 8147−8154.

(13) Liu, J. W. DNA-Stabilized, Fluorescent, Metal Nanoclusters for Biosensor Development. *Trac-Trends Anal. Chem.* **2014**, *58*, 99−111.

(14) Han, J. H.; Tan, M.; Sudheendra, L.; Weiss, R. H.; Kennedy, I. M. On-Chip Detection of a Single Nucleotide Polymorphism without Polymerase Amplification. *Nano Res.* **2014**, *7*, 1302−1310.

(15) Wen, Y.; Li, F. Y.; Dong, X.; Zhang, J.; Xiong, Q.; Chen, P. The Electrical Detection of Lead Ions Using Gold-Nanoparticle and Dnazyme-Functionalized Graphene Device. *Adv. Healthcare Mater.* **2013**, *2*, 271−274.

(16) Dong, X. C.; Xu, H.; Wang, X. W.; Huang, Y. X.; Chan-Park, M. B.; Zhang, H.; Wang, L.-H.; Huang, W.; Chen, P. 3D Graphene-Cobalt Oxide Electrode for High-Performance Supercapacitor and Enzyme-less Glucose Detection. *ACS Nano* **2012**, *6*, 3206−3213.

(17) Yang, X.; Li, J.; Pei, H.; Li, D.; Zhao, Y.; Gao, J.; Lu, J.; Shi, J.; Fan, C.; Huang, Q. Pattern Recognition Analysis of Proteins Using DNA-Decorated Catalytic Gold Nanoparticles. *Small* **2013**, *9*, 2844−2849.

(18) Wang, P.; Pei, H.; Wan, Y.; Li, J.; Zhu, X.; Su, Y.; Fan, C.; Huang, Q. Nanomechanical Identification of Proteins Using Mmicrocantilever-Based Chemical Sensors. *Nanoscale* **2012**, *4*, 6739−6742.

(19) Perea-López, N.; Elías, A. L.; Berkdemir, A.; Castro-Beltran, A.; Gutiérrez, H. R.; Feng, S.; Lv, R.; Hayashi, T.; López-Urías, F.; Ghosh, S. Photosensor Device Based on Few-Layered WS2 Films. *Adv. Funct. Mater.* **2013**, *23*, 5511−5517.

(20) Jaramillo, T. F.; Jørgensen, K. P.; Bonde, J.; Nielsen, J. H.; Horch, S.; Chorkendorff, I. Identification of Active Edge Sites for Electrochemical H_2 Evolution from MoS_2 Nanocatalysts. *Science* **2007**, *317*, 100−102.

(21) Peng, H.; Lai, K.; Kong, D.; Meister, S.; Chen, Y.; Qi, X.-L.; Zhang, S.-C.; Shen, Z.-X.; Cui, Y. Aharonov-Bohm Interference in Topological Insulator Nanoribbons. *Nat. Mater.* **2010**, *9*, 225−229.

(22) Radisavljevic, B.; Radenovic, A.; Brivio, J.; Giacometti, V.; Kis, A. Single-Layer MoS2 Transistors. *Nat. Nanotechnol.* **2011**, *6*, 147−150.

(23) Chhowalla, M.; Shin, H. S.; Eda, G.; Li, L.-J.; Loh, K. P.; Zhang, H. The Chemistry of Two-Dimensional Layered Transition Metal Dichalcogenide Nanosheets. *Nat. Chem.* **2013**, *5*, 263−275.

(24) Liu, T.; Wang, C.; Cui, W.; Gong, H.; Liang, C.; Shi, X.; Li, Z.; Sun, B.; Liu, Z. Combined Photothermal and Photodynamic Therapy Delivered by PEGylated MoS_2 Nanosheets. *Nanoscale* **2014**, *6*, 11219−11225.

(25) Liu, T.; Wang, C.; Gu, X.; Gong, H.; Cheng, L.; Shi, X.; Feng, L.; Sun, B.; Liu, Z. Drug Delivery with PEGylated MoS_2 Nano-sheets for Combined Photothermal and Chemotherapy of Cancer. *Adv. Mater.* **2014**, *26*, 3433−3440.

(26) Cheng, L.; Liu, J.; Gu, X.; Gong, H.; Shi, X.; Liu, T.; Wang, C.; Wang, X.; Liu, G.; Xing, H. PEGylated WS_2 Nanosheets as a Multifunctional Theranostic Agent for in vivo Dual-Modal CT/Photoacoustic Imaging Guided Photothermal Therapy. *Adv. Mater.* **2014**, *26*, 1886−1893.

(27) Wang, H.; Dai, H. Strongly Coupled Inorganic-Nano-Carbon Hybrid Materials for Energy Storage. *Chem. Soc. Rev.* **2013**, *42*, 3088−3113.

(28) Choi, C.; Feng, J.; Li, Y. G.; Wu, J.; Zak, A.; Tenne, R.; Dai, H. J. WS_2 Nanoflakes from Nanotubes for Electrocatalysis. *Nano Res.* **2013**, *6*, 921−928.

(29) Buscema, M.; Steele, G. A.; van der Zant, H. S. J.; Castellanos-Gomez, A. The Effect of the Substrate on the Raman and Photoluminescence Emission of Single-Layer MoS_2. *Nano Res.* **2014**, *7*, 561−571.

(30) Li, X.; Qi, W.; Mei, D.; Sushko, M. L.; Aksay, I.; Liu, J. Functionalized Graphene Sheets as Molecular Templates for Controlled Nucleation and Self-Assembly of Metal Oxide-Graphene Nanocomposites. *Adv. Mater.* **2012**, *24*, 5136−5141.

(31) Zhu, C.; Zeng, Z.; Li, H.; Li, F.; Fan, C.; Zhang, H. Single-Layer MoS_2-Based Nanoprobes for Homogeneous Detection of Biomolecules. *J. Am. Chem. Soc.* **2013**, *135*, 5998−6001.

(32) Wang, L.; Wang, Y.; Wong, J. I.; Palacios, T.; Kong, J.; Yang, H. Y. Functionalized MoS_2 Nanosheet-Based Field-Effect Biosensor for Label-Free Sensitive Detection of Cancer Marker Proteins in Solution. *Small* **2014**, *10*, 1101−1105.

(33) Wang, Y.; Ni, Y. N. Molybdenum Disulfide Quantum Dots as a Photoluminescence Sensing Platform for 2,4,6-Trinitrophenol Detection. *Anal. Chem.* **2014**, *86*, 7463−7470.

(34) Sarkar, D.; Liu, W.; Xie, X. J.; Anselmo, A. C.; Mitragotri, S.; Banerjee, K. MoS_2 Field-Effect Transistor for Next-Generation Label-Free Biosensors. *ACS Nano* **2014**, *8*, 3992−4003.

(35) Lin, T. R.; Zhong, L. S.; Song, Z. P.; Guo, L. Q.; Wu, H. Y.; Guo, Q. Q.; Chen, Y.; Fu, F. F.; Chen, G. N. Visual Detection of Blood Glucose Based on Peroxidase-Like Activity of WS_2 Nanosheets. *Biosens. Bioelectron.* **2014**, *62*, 302−307.

(36) Farimani, A. B.; Min, K.; Aluru, N. R. DNA Base Detection Using a Single-Layer MoS_2. *ACS Nano* **2014**, *8*, 7914−7922.

(37) Xi, Q.; Zhou, D.-M.; Kan, Y.-Y.; Ge, J.; Wu, Z.-K.; Yu, R.-Q.; Jiang, J.-H. Highly Sensitive and Selective Strategy for MicroRNA Detection Based on WS_2 Nanosheet Mediated Fluorescence Quenching and Duplex-Specific Nuclease Signal Amplification. *Anal. Chem.* **2014**, *86*, 1361−1365.

(38) Loan, P. T. K.; Zhang, W. J.; Lin, C. T.; Wei, K. H.; Li, L. J.; Chen, C. H. Graphene/MoS_2 Heterostructures for Ultrasensitive Detection of DNA Hybridisation. *Adv. Mater.* **2014**, *26*, 4838.

DOI: 10.1021/acsami.5b01222
ACS Appl. Mater. Interfaces 2015, 7, 7526−7533

(39) Cheng, L.; Liu, J.; Gu, X.; Gong, H.; Shi, X.; Liu, T.; Wang, C.; Wang, X.; Liu, G.; Xing, H.; Bu, W.; Sun, B.; Liu, Z. PEGylated WS_2 Nanosheets as a Multifunctional Theranostic Agent for in vivo Dual-Modal CT/Photoacoustic Imaging Guided Photothermal Therapy. *Adv. Mater.* **2014**, *26*, 1886−1893.
(40) Chou, S. S.; De, M.; Kim, J.; Byun, S.; Dykstra, C.; Yu, J.; Huang, J.; Dravid, V. P. Ligand Conjugation of Chemically Exfoliated MoS_2. *J. Am. Chem. Soc.* **2013**, *135*, 4584−4587.
(41) Zhang, J.; Malicka, J.; Gryczynski, I.; Lakowicz, J. R. Surface-Enhanced Fluorescence of Fluorescein-Labeled Oligonucleotides Capped on Silver Nanoparticles. *J. Phys. Chem. B* **2005**, *109*, 7643−7648.
(42) Russell, K. J.; Liu, T.-L.; Cui, S.; Hu, E. L. Large Spontaneous Emission Enhancement in Plasmonic Nanocavities. *Nat. Photonics* **2012**, *6*, 459−462.
(43) Brolo, A. G. Plasmonics for Future Biosensors. *Nat. Photonics* **2012**, *6*, 709−713.
(44) Hong, G.; Tabakman, S. M.; Welsher, K.; Wang, H.; Wang, X.; Dai, H. Metal-Enhanced Fluorescence of Carbon Nanotubes. *J. Am. Chem. Soc.* **2010**, *132*, 15920−15923.
(45) Hong, G.; Tabakman, S. M.; Welsher, K.; Chen, Z.; Robinson, J. T.; Wang, H.; Zhang, B.; Dai, H. Near-Infrared-Fluorescence-Enhanced Molecular Imaging of Live Cells on Gold Substrates. *Angew. Chem. Int. Ed.* **2011**, *50*, 4644−4648.
(46) Ling, X.; Fang, W.; Lee, Y.-H.; Araujo, P. T.; Zhang, X.; Rodriguez-Nieva, J. F.; Lin, Y.; Zhang, J.; Kong, J.; Dresselhaus, M. S. Raman Enhancement Effect on Two-Dimensional Layered Materials: Graphene, h-BN and MoS_2. *Nano Lett.* **2014**, *14*, 3033−3040.
(47) Freeman, R.; Finder, T.; Willner, I. Multiplexed Analysis of Hg^{2+} and Ag^{+} Ions by Nucleic Acid Functionalized CdSe/ZnS Quantum Dots and Their Use for Logic Gate Operations. *Angew. Chem. Int. Ed.* **2009**, *48*, 7818−7821.
(48) Lin, C.-Y.; Yu, C.-J.; Lin, Y.-H.; Tseng, W.-L. Colorimetric Sensing of Silver(I) and Mercury(II) Ions Based on an Assembly of Tween 20-Stabilized Gold Nanoparticles. *Anal. Chem.* **2010**, *82*, 6830−6837.
(49) Tan, E.; Yin, P.; Lang, X.; Wang, X.; You, T.; Guo, L. Functionalized Gold Nanoparticles as Nanosensor for Sensitive and Selective Detection of Silver Ions and Silver Nanoparticles by Surface-Enhanced Raman Scattering. *Analyst* **2012**, *137*, 3925−3928.
(50) Yang, H. C.; Liu, X. X.; Fei, R. H.; Hu, Y. G. Sensitive and Selective Detection of Ag^{+} in Aqueous Solutions Using Fe_3O_4@Au Nanoparticles as Smart Electrochemical Nanosensors. *Talanta* **2013**, *116*, 548−553.
(51) Huang, H.; Chen, S.; Liu, F.; Zhao, Q.; Liao, B.; Yi, S.; Zeng, Y. Multiplex Plasmonic Sensor for Detection of Different Metal Ions Based on a Single Type of Gold Nanorod. *Anal. Chem.* **2013**, *85*, 2312−2319.
(52) Huang, H.; Qu, C.; Liu, X.; Huang, S.; Xu, Z.; Liao, B.; Zeng, Y.; Chu, P. K. Preparation of Controllable Core-Shell Gold Nanoparticles and Its Application in Detection of Silver Ions. *ACS Appl. Mater. Interfaces* **2011**, *3*, 183−190.
(53) Liang, J. G.; Ai, X. P.; He, Z. K.; Pang, D. W. Functionalized CdSe Quantum Dots as Selective Silver Ion Chemodosimeter. *Analyst* **2004**, *129*, 619−622.
(54) Zhang, B. H.; Qi, L.; Wu, F. Y. Functionalized Manganese-Doped Zinc Sulfide Core/Shell Quantum Dots as Selective Fluorescent Chemodosimeters for Silver Ion. *Microchim. Acta* **2010**, *170*, 147−153.
(55) Lin, C. Y.; Yu, C. J.; Lin, Y. H.; Tseng, W. L. Colorimetric Sensing of Silver (I) and Mercury (II) Ions Based on an Assembly of Tween 20-Stabilized Gold Nanoparticles. *Anal. Chem.* **2010**, *82*, 6830−6837.
(56) Chen, X.; Chen, Y. R.; Zhou, X. D.; Hu, J. M. Detection of Ag^{+} Ions and Cysteine Based on Chelation Actions Between Ag^{+} Ions and Guanine Bases. *Talanta* **2013**, *107*, 277−283.

DOI: 10.1021/acsami.5b01222
ACS Appl. Mater. Interfaces 2015, 7, 7526−7533